研究成果の刊行に関する一覧表

研究成果の刊行に関する一覧表（服部　信孝）

雑誌

発表者氏名	論文タイトル名	発表誌名	巻号	ページ	出版年
Saiki S, Sasazawa Y, Imamichi Y, Kawajiri S, Fujimaki T, Tanida I, Kobayashi H, Sato F, Kei-Ichi Ishikawa, Sato S, Imoto M, Hattori N.	Caffeine induces apoptosis by enhancement of autophagy via PI3K/Akt/mTOR/p70S6K inhibition.	***Autophagy***	7	176-87	2011
Amo T, Sato S, Saiki S, Wolf AM, Toyomizu M, Gautier CA, Shen J, Ohta S, Hattori N.	Mitochondrial membrane potential decrease caused by loss of PINK1 is not due to proton leak, but to respiratory chain defects.	***Neurobiol Dis***	41	111-8	2011
Kawajiri S, Saiki S, Sato S, Hattori N	Genetic mutations and functions of PINK1.	***Trends Pharmacol Sci***	32	573-80	2011
Usami Y, Hatano T, Imai S, Kubo S, Sato S, Saiki S, Fujioka Y, Ohba Y, Sato F, Funayama M, Eguchi H, Shiba K, Ariga H, Shen J, Hattori N.	DJ-1 associates with synaptic membranes.	***Neurobiol Dis***	43	651-62	2011
Saiki S, Sato S, Hattori N.	Molecular pathogenesis of Parkinson disease: update.	***J Neurol Neurosurg Psychiat***	83	430-6	2012

研究成果の刊行に関する一覧表（佐藤　栄人）

雑誌

発表者氏名	論文タイトル名	発表誌名	巻号	ページ	出版年
Saiki S, Sasazawa Y, Imamichi Y, Kawajiri S, Fujimaki T, Tanida I, Kobayashi H, Sato F, Kei-Ichi Ishikawa, Sato S, Imoto M, Hattori N.	Caffeine induces apoptosis by enhancement of autophagy via PI3K/Akt/mTOR/p70S6K inhibition.	***Autophagy***	7	176-87	2011
Amo T, Sato S, Saiki S, Wolf AM, Toyomizu M, Gautier CA, Shen J, Ohta S, Hattori N.	Mitochondrial membrane potential decrease caused by loss of PINK1 is not due to proton leak, but to respiratory chain defects.	***Neurobiol Dis***	41	111-8	2011
Kawajiri S, Saiki S, Sato S, Hattori N	Genetic mutations and functions of PINK1.	***Trends Pharmacol Sci***	32	573-80	2011
Usami Y, Hatano T, Imai S, Kubo S, Sato S, Saiki S, Fujioka Y, Ohba Y, Sato F, Funayama M, Eguchi H, Shiba K, Ariga H, Shen J, Hattori N.	DJ-1 associates with synaptic membranes.	***Neurobiol Dis***	43	651-62	2011
Saiki S, Sato S, Hattori N.	Molecular pathogenesis of Parkinson disease: update.	***J Neurol Neurosurg Psychiat***	83	430-6	2012

研究成果の刊行に関する一覧表（斉木　臣二）

雑誌

発表者氏名	論文タイトル名	発表誌名	巻号	ページ	出版年
Saiki S, Sasazawa Y, Imamichi Y, Kawajiri S, Fujimaki T, Tanida I, Kobayashi H, Sato F, Kei-Ichi Ishikawa, Sato S, Imoto M, Hattori N.	Caffeine induces apoptosis by enhancement of autophagy via PI3K/Akt/mTOR/p70S6K inhibition.	***Autophagy***	7	176-87	2011
Amo T, Sato S, Saiki S, Wolf AM, Toyomizu M, Gautier CA, Shen J, Ohta S, Hattori N.	Mitochondrial membrane potential decrease caused by loss of PINK1 is not due to proton leak, but to respiratory chain defects.	***Neurobiol Dis***	41	111-8	2011
Kawajiri S, Saiki S, Sato S, Hattori N	Genetic mutations and functions of PINK1.	***Trends Pharmacol Sci***	32	573-80	2011
Usami Y, Hatano T, Imai S, Kubo S, Sato S, Saiki S, Fujioka Y, Ohba Y, Sato F, Funayama M, Eguchi H, Shiba K, Ariga H, Shen J, Hattori N.	DJ-1 associates with synaptic membranes.	***Neurobiol Dis***	43	651-62	2011
Saiki S, Sato S, Hattori N.	Molecular pathogenesis of Parkinson disease: update.	***J Neurol Neurosurg Psychiat***	83	430-6	2012

研究成果の刊行に関する一覧表（井本　正哉）

雑誌

発表者氏名	論文タイトル名	発表誌名	巻号	ページ	出版年
H. Kobayashi, H. Harada, M. Nakamura, Y. Futamura, A. Ito, M. Yoshida, S. Iemura, K. Shin-ya, T. Doi, T. Takahashi, T. Natsume, M. Imoto and Y. Sakakibara.	Comprehensive Predictions of Target Proteins Based on Protein-Chemical Interaction Using Virtual Screening and Experimental Verifications.	***BMC Chemical Biology,***		In press	2012
Y. Sasazawa, S. Kanagaki, E. Tashiro, T. Nogawa, M. Muroi, Y. Kondoh, H. Osada & M. Imoto	Xanthohumol impairs autophagosome maturation through direct inhibition of valosin-containing protein.	***ACS Chemical Biology***		In press	2012
K. Yamamoto, M. Makino, R. Watanapokasin, E. Tashiro & M. Imoto	Inostamycin enhanced TRAIL-induced apoptosis through DR5 up-regulation on the cell surface	***Journal of Antibiotics***		In press	2012
E. Tashiro & M. Imoto	Target identification of bioactive compounds.	***Bioorganic & Medicinal Chemistry***	20	1910-1921	2012
K. Yamamoto, E. Tashiro, K. Motohashi, H. Seto & M. Imoto	Napyradiomycin A1, an inhibitor of mitochondrial complexes I and II.	***The Journal of Antibiotics***	65	211-214	2012
H. Kobayashi, Y. Ogura, M. Sawada, R. Nakayama, K. Takano, Y. Minato, Y. Takemoto, E. Tashiro, H. Watanabe & M. Imoto	Involvement of 14-3-3 proteins in the second epidermal growth factor-induced wave of Rac1 activation in the process of cell migration.	***The Journal of Biological Chemistry***	286	39259 –39268	2011
Y. Yamada, E. Tashiro, S. Taketani, M. Imoto & T. Kataoka	Mycotrienin II, a translation inhibitor that prevents ICAM-1 expression induced by pro-inflammatory cytokines.	***The Journal of Antibiotics***	64	361-366	2011

T. Kawamura, K. Matsubara, H, Otaka, E. Tashiro, K. Shindo, R. C. Yanagita, K. Irie, and M. Imoto	Generation of "Unnatural Natural Product" library and identification of a small molecule inhibitor of XIAP.	***Bioorganic & Medicinal Chemistry***		In press	2011
M. Sawada, S. Kubo, K. Matsumura, Y. Takemoto, H. Kobayashi, E. Tashiro, T. Kitahara, H. Watanabe and M. Imoto	Synthesis and anti-migrative evaluation of moverastin derivatives.	***Bioorganic & Medicinal Chemistry Letters.***	21	1385-1389	2011
K. Yamamoto, E. Tashiro and M. Imoto	Quinotrierixin Inhibits ER Stress-induced XBP1 mRNA Splicing through Inhibition of Protein Synthesis.	***Biosci. Biotechnol. Biochem.***	75	284-288	2011
M. Kitagawa, M. Misawa, S. Ogawa, E. Tashiro and M. Imoto	A New Convenient Cell-based Screening Method for Small Molecule Glycolytic Inhibitors.	***Biosci. Biotechnol. Biochem.***	75	367-369	2011
S. Saiki, Y. Sasazawa, Y. Imamichi, S. Kawajiri, T. Fujimaki, I. Tanida, H. Kobayashi, F. Sato, S. Sato, K. Ishikawa, M. Imoto and N. Hattori	Caffeine induces apoptosis by enhancement of autophagy via PI3K/Akt/mTOR/p70S6K inhibition.	***Autophagy***	7	42-53	2011

研究成果の刊行に関する一覧表（田代　悦）

雑誌

発表者氏名	論文タイトル名	発表誌名	巻号	ページ	出版年
K. Yamamoto, M. Makino, R. Watanapokasin, E. Tashiro & M. Imoto	Inostamycin enhanced TRAIL-induced apoptosis through DR5 up-regulation on the cell surface	***Journal of Antibiotics***		In press	2012
Y. Sasazawa, S. Kanagaki, E. Tashiro, T. Nogawa, M. Muroi, Y. Kondoh, H. Osada & M. Imoto	Xanthohumol impairs autophagosome maturation through direct inhibition of valosin-containing protein.	***ACS Chemical Biology***		In press	2012
K. Yamamoto, E. Tashiro, K. Motohashi, H. Seto & M. Imoto	Napyradiomycin A1, an inhibitor of mitochondrial complexes I and II.	***The Journal of Antibiotics***	65	211-214	2012
M. Kiga, F. Tanzawa, S. Iwasaki, F. Inaba, K. Fujiwara, H. Iwadare, T. Echigo, Y. Nakamura, T. Shibata, K. Suzuki, I.Yasumatsu, A.Nakayama, Y. Sasazawa, E. Tashiro, M. Imoto & S. Kurakata	Antitumor effects of novel highly hydrophilic and non-ATP-competitive MEK1/2 inhibitor, SMK-17.	***Anti-cancer drugs***	23	119-130	2012
E. Tashiro & M. Imoto	Target identification of bioactive compounds.	***Bioorganic & Medicinal Chemistry***	20	1910-1921	2012
H. Kobayashi, Y. Ogura, M. Sawada, R. Nakayama, K. Takano, Y. Minato, Y. Takemoto, E. Tashiro, H. Watanabe & M. Imoto	Involvement of 14-3-3 proteins in the second epidermal growth factor-induced wave of Rac1 activation in the process of cell migration.	***The Journal of Biological Chemistry***	286	39259 –39268	2011
Y. Yamada, E. Tashiro, S. Taketani, M. Imoto & T. Kataoka	Mycotrienin II, a translation inhibitor that prevents ICAM-1 expression induced by pro-inflammatory cytokines.	***The Journal of Antibiotics***	64	361-366	2011

研究成果の刊行物・別刷り

Neurobiology of Disease 41 (2011) 111–118

Contents lists available at ScienceDirect

Neurobiology of Disease

journal homepage: www.elsevier.com/locate/ynbdi

Mitochondrial membrane potential decrease caused by loss of PINK1 is not due to proton leak, but to respiratory chain defects

Taku Amo [a,1], Shigeto Sato [b], Shinji Saiki [b], Alexander M. Wolf [a], Masaaki Toyomizu [c], Clement A. Gautier [d], Jie Shen [d], Shigeo Ohta [a], Nobutaka Hattori [b,*]

[a] Department of Biochemistry and Cell Biology, Institute of Development and Aging Sciences, Graduate School of Medicine, Nippon Medical School, 1-396 Kosugi-cho, Nakahara-ku, Kawasaki 211-8533, Japan
[b] Department of Neurology, Juntendo University School of Medicine, 2-1-1 Hongo, Bunkyo-ku, Tokyo 113-8421, Japan
[c] Animal Nutrition, Life Sciences, Graduate School of Agricultural Science, Tohoku University, 1-1 Tsutsumidori-Amamiyamachi, Aoba-ku, Sendai 981-8555, Japan
[d] Center for Neurologic Diseases, Brigham and Women's Hospital, Program in Neuroscience, Harvard Medical School, Boston, MA 02115, USA

ARTICLE INFO

Article history:
Received 29 June 2010
Revised 17 August 2010
Accepted 25 August 2010
Available online 15 September 2010

Keywords:
Parkinson's disease
Mitochondria
PINK1
Parkin
Membrane potential
Oxidative phosphorylation
Modular kinetic analysis
Proton leak
Reactive oxygen species

ABSTRACT

Mutations in *PTEN-induced putative kinase 1* (*PINK1*) cause a recessive form of Parkinson's disease (PD). PINK1 is associated with mitochondrial quality control and its partial knock-down induces mitochondrial dysfunction including decreased membrane potential and increased vulnerability against mitochondrial toxins, but the exact function of PINK1 in mitochondria has not been investigated using cells with null expression of PINK1. Here, we show that loss of PINK1 caused mitochondrial dysfunction. In PINK1-deficient ($PINK1^{-/-}$) mouse embryonic fibroblasts (MEFs), mitochondrial membrane potential and cellular ATP levels were decreased compared with those in littermate wild-type MEFs. However, mitochondrial proton leak, which reduces membrane potential in the absence of ATP synthesis, was not altered by loss of PINK1. Instead, activity of the respiratory chain, which produces the membrane potential by oxidizing substrates using oxygen, declined. H_2O_2 production rate by $PINK1^{-/-}$ mitochondria was lower than $PINK1^{+/+}$ mitochondria as a consequence of decreased oxygen consumption rate, while the proportion (H_2O_2 production rate per oxygen consumption rate) was higher. These results suggest that mitochondrial dysfunctions in PD pathogenesis are caused not by proton leak, but by respiratory chain defects.

Introduction

Parkinson's disease (PD) is a neurodegenerative disease characterized by loss of dopaminergic neurons in the substantia nigra. Mitochondrial dysfunction has been proposed as a major factor in the pathogenesis of sporadic and familial PD (Abou-Sleiman et al., 2006). In particular, the identification of mutations in *PTEN-induced putative kinase 1* (*PINK1*) has strongly implicated mitochondrial dysfunction owing to its loss of function in the pathogenesis of PD (Valente et al., 2004). PINK1 contains an N-terminal mitochondrial targeting sequence (MTS) and a serine/threonine kinase domain (Valente et al., 2004). PINK1 kinase activity is crucial for mitochondrial maintenance via TRAP phosphorylation (Pridgeon et al., 2007). Loss of PINK1 function induces increased vulnerability to various stresses (Exner et al., 2007; Haque et al., 2008; Pridgeon et al., 2007; Wood-Kaczmar et al., 2008). However, silencing of PINK1 has only been partial and only one study has been performed to assess mitochondrial functions in steady and artificial states with complete ablation of PINK1 expression (Gautier et al., 2008).

Several studies have shown that PINK1 acts upstream of parkin in the same genetic pathway (Clark et al., 2006; Park et al., 2006) and co-overexpressed PINK1 and parkin both co-localized to mitochondria (Kim et al., 2008). Overexpression of PINK1 promotes mitochondrial fission (Yang et al., 2008). Fission followed by selective fusion segregates dysfunctional mitochondria and permits their removal by autophagy (Twig et al., 2008). PINK1 loss-of-function decreases mitochondrial membrane potential (Chu, 2010) and the PINK1–parkin pathway is associated with mitochondrial elimination in cultured cells treated with the mitochondrial uncoupler carbonyl cyanide *m*-chlorophenylhydrazone (CCCP), which causes mitochondrial depolarization (Geisler et al., 2010; Kawajiri et al., 2010; Matsuda et al., 2010; Narendra et al., 2008, 2010; Vives-Bauza et al., 2010). However, the exact mechanism underlying the mitochondrial depolarization induced by PINK1 defects leading to mitochondrial autophagy has not been examined in detail.

Abbreviations: $\Delta\psi$, mitochondrial membrane potential; FCCP, carbonyl cyanide *p*-trifluoromethoxyphenylhydrazone; MEFs, mouse embryonic fibroblasts; PD, Parkinson's disease; PINK1, PTEN-induced putative kinase 1; ROS, reactive oxygen species; TMRM, tetramethylrhodamine methyl ester; TPMP, triphenylmethylphosphonium.

* Corresponding author. Fax: +81 3 5800 0547.
E-mail address: nhattori@juntendo.ac.jp (N. Hattori).
[1] Present address: Department of Applied Chemistry, National Defense Academy, 1-10-20 Hashirimizu, Yokosuka 239-8686, Japan.

Available online on ScienceDirect (www.sciencedirect.com).

0969-9961/$ – see front matter © 2010 Elsevier Inc. All rights reserved.
doi:10.1016/j.nbd.2010.08.027

Here, we describe a detailed characterization of mitochondria in PINK1-deficient cells. We show that PINK1 deficiency causes a decrease in mitochondrial membrane potential, which is not due to proton leak, but to respiratory chain defects.

Materials and methods

PINK1 knock-out mouse embryonic fibroblasts (MEFs)

PINK1 knock-out MEFs were prepared and cultured as described previously (Matsuda et al., 2010). Mouse embryonic fibroblasts (MEFs) were derived from E12.5 embryos containing littermate 4 mice of each genotype. Embryos were mechanically dispersed by repeated passage through a P1000 pipette tip and plated with MEF media containing DME, 10% FCS, 1× nonessential amino acids, 1 mM L-glutamine, penicillin/streptomycin (invitrogen). The ψ2 cell line, an ecotropic retrovirus packaging cell line, was maintained in Dulbecco's modified Eagle medium (DMEM, Sigma) with 5% fetal bovine serum and 50 μg/ml kanamicin. Transfection of the ψ2 cells with pMESVTS plasmids containing an SV40 large T antigen was performed by lipofection method according to the manual provided by the manufacturer (GIBCO BRL). Five micrograms of the plasmids was used for each transfection. Transfectants were selected by G418 at the concentration of 0.5 mg/ml, and 10 clonal cell lines were established. The highest titer of 5×10^4 cfu/ml was obtained for the conditioned medium of a cell line designated ψ2SVTS1. 10^6 MEFs were plated onto a 10-cm culture dish and kept at 33 °C for 48 hours. Then medium was replaced with 2 ml supplemented with polybrene-supplemented medium conditioned by the ψ2SVTS1 cells at confluency for 3 days. Infection was continued for 3 hours, and the medium was replaced with a fresh one. The infected MEFs were cultured at 33 °C until immortalized cells were obtained.

We confirmed that the differences we detected in this study were due to the PINK1 deficiency, not to artificial effects by immortalization, by measuring cellular respiration rates of not immortalized MEFs from other littermates (Supplemental figure). The respiration rates of not immortalized MEFs were slightly slower than those of immortalized MEFs, but the differences between PINK1$^{+/+}$ and $^{-/-}$ MEFs were consistent (Fig. 2A).

Cell growth

Cells were seeded in 12-well plates at density of $3\sim6\times10^3$ cells/well and incubated in DMEM high glucose medium (4.5 g/l glucose and 1 mM sodium pyruvate) supplemented with 10% fetal bovine serum. After a day, the medium was replaced with DMEM glucose-free medium supplemented with 1 g/l galactose, 1 mM sodium pyruvate and 10% fetal bovine serum (DMEM galactose medium) at 37 °C in an incubator with a humidified atmosphere of 5% CO_2. Cells were trypsinized and live cells were assessed by trypan blue dye exclusion.

Mitochondrial morphological changes

Cells were seeded in 6-well plates at 2.0×10^5/well and incubated in DMEM high glucose medium (4.5 g/l glucose and 1 mM sodium pyruvate) supplemented with 10% fetal bovine serum and 1% penicillin/streptomycin. After a day, the medium was replaced with DMEM glucose-free medium supplemented with 1 g/l galactose, 1 mM sodium pyruvate and 10% fetal bovine serum (DMEM galactose medium) at 37 °C in an incubator with a humidified atmosphere of 5% CO_2. 24 hours later, cells were fixed and immunostained with anti-Tom20 antibody to visualize mitochondria according to a protocol as previously described (Kawajiri et al., 2010). All images were obtained using an Axioplan 2 imaging microscope (Carl Zeiss, Oberkochen, Germany).

Cellular ATP levels

Intracellular ATP levels were determined by a cellular ATP assay kit (TOYO B-Net, Tokyo, Japan) according to the manufacturer's instructions using a Lumat LB9507 luminometer (Berthold Technology, Bad Wildbad, Germany).

Membrane potential

Fluorescence images were recorded using a multi-dimensional imaging workstation (AS MDW, Leica Microsystems, Wetzlar, Germany) with a climate chamber maintained at 37 °C. Fluorescence was quantified with a CCD camera (CoolSnap HQ, Roper Scientific, Princeton, NJ) using a 20× objective. Cells were stained for 1 hour with a non-quenching concentration (20 nM) of tetramethylrhodamine methyl ester (TMRM) in a 96-well plate. The cell-permeable cationic dye TMRM accumulates in mitochondria according to the Nernst equation. Nuclei were stained with 250 nM Hoechst 34580. Mitochondrial TMRM fluorescence was integrated in a 40-μm diameter circular area around the nucleus, and the minimum fluorescence in this area was subtracted as background fluorescence.

Cell respiration

Cell respiration was measured at 37 °C using the Oxygen Meter Model 781 and the Mitocell MT200 closed respiratory chamber (Strathkelvin Instruments, North Lanarkshire, United Kingdom). Cells were cultured in DMEM with 4.5 g/l of glucose supplemented with 10% FBS. Cells were then trypsinized and resuspended in Leibovitz's L-15 medium (Invitrogen) at density of 8.0×10^6 cells/ml. The oxygen respiration rate was measured under each of the following three conditions: basal rate (no additions); State 4 (no ATP synthesis) [after addition of 1 μg/ml oligomycin (Sigma)], uncoupled [after addition of 3 μM FCCP (carbonyl cyanide *p*-trifluoromethoxyphenylhydrazone; Sigma)] using Strathkelvin 949 Oxygen System. After sequential measurements, the endogenous respiration rate was determined by adding 1 μM rotenone + 2 μM myxothiazol.

Mitochondrial respiration and membrane potential

Mitochondria were prepared from cultured MEFs as previously described (Amo and Brand, 2007). Mitochondrial oxygen consumption with 5 mM succinate as a respiratory substrate was measured at 37 °C using a Clark electrode (Rank Brothers, Cambridge, United Kingdom) calibrated with air-saturated respiration buffer comprising 0.115 M KCl, 10 mM KH_2PO_4, 3 mM HEPES (pH 7.2), 2 mM $MgCl_2$, 1 mM EGTA and 0.3% (w/v) defatted BSA, assumed to contain 406 nmol atomic oxygen/ml (Reynafarje et al., 1985). Mitochondrial membrane potential ($\Delta\psi$) was measured simultaneously with respiratory activity using an electrode sensitive to the lipophilic cation $TPMP^+$ (triphenylmethylphosphonium) (Brand, 1995). Mitochondria were incubated at 0.5 mg/ml in the presence of 80 ng/ml nigericin (to collapse the pH gradient so that the proton motive force was expressed exclusively as $\Delta\psi$) and 2 μM rotenone (to inhibit complex I). The $TPMP^+$-sensitive electrode was calibrated with sequential additions of $TPMP^+$ up to 2 μM, then 5 mM succinate was added to initiate respiration. Experiments were terminated with 2 μM FCCP, allowing correction for any small baseline drift. $\Delta\psi$ was calculated from the distribution of $TPMP^+$ across the mitochondrial inner membrane using a binding correction factor of 0.35 mg protein/μl. Respiratory rates with 4 mM pyruvate + 1 mM malate as a substrate in State 3 (with 0.25 mM ADP) and State 4 (with 1 μg/ml oligomycin) were determined using the Oxygen Meter Model 781 and the Mitocell MT200 closed respiratory chamber (Strathkelvin Instruments).

Modular kinetic analysis

To investigate differences in oxidative phosphorylation caused by PINK1 knock-out, we applied a systems approach, namely modular kinetic analysis (Amo and Brand, 2007; Brand, 1990). This analyzes the kinetics of the whole of oxidative phosphorylation divided into three modules connected by their common substrate or product, $\Delta\psi$. The modules are (i) the reactions that produce $\Delta\psi$, consisting of the substrate translocases, dehydrogenases and other enzymes and the components of the respiratory chain, called 'substrate oxidation'; (ii) the reactions that consume $\Delta\psi$ and synthesize, export and dephosphorylate ATP, consisting of ATP synthase, the phosphate and adenine nucleotide translocases and any ATPases that may be present, called the 'phosphorylating system'; and (iii) the reactions that consume $\Delta\psi$ without ATP synthesis, called the 'proton leak' (Brand, 1990). The analysis reports changes anywhere within oxidative phosphorylation that are functionally important but is unresponsive to changes that have no functional consequences. Comparison of the kinetic responses of each of the three modules to $\Delta\psi$ obtained using mitochondria isolated from PINK1$^{+/+}$ and PINK1$^{-/-}$ MEFs would reveal any effects of PINK1 on the kinetics of oxidative phosphorylation. Oxygen consumption and $\Delta\psi$ were measured simultaneously using mitochondria incubated with 80 ng/ml nigericin and 4 μM rotenone. Respiration was initiated by 5 mM succinate. The kinetic behavior of a '$\Delta\psi$-producer' can be established by specific modulation of a $\Delta\psi$-consumer and the kinetics of a consumer can be established by specific modulation of a $\Delta\psi$-producer (Brand, 1998). To measure the kinetic response of proton leak to $\Delta\psi$, the State 4 (non-phosphorylating) respiration of mitochondria in the presence of oligomycin (0.8 μg/ml; to prevent any residual ATP synthesis), which was used solely to drive the proton leak, was titrated with malonate (up to 8 mM). In a similar way, State 4 respiration was titrated by FCCP (up to 1 μM) for measurement of the kinetic response of substrate oxidation to $\Delta\psi$. State 3 (maximal rate of ATP synthesis) was obtained by addition of excess ADP (1 mM). Titration of State 3 respiration with malonate (up to 1.1 mM) allowed measurement of the kinetics of the $\Delta\psi$-consumers (the sum of the phosphorylating system and proton leak). The coupling efficiencies of oxidative phosphorylation were calculated from the kinetic curves as the percentage of mitochondrial respiration rate at a given $\Delta\psi$ that was used for ATP synthesis and was therefore inhibited by oligomycin. Note that any slip reactions will appear as proton leak in this analysis (Brand et al., 1994).

Mitochondrial ROS production

Mitochondrial ROS production rate was assessed by measurement of H_2O_2 generation rate, determined fluorometrically by measurement of oxidation of Amplex Red to fluorescent resorufin coupled to the enzymatic reduction of H_2O_2 by horseradish peroxidase using a spectrofluorometer RF-5300PC (Shimadzu, Kyoto, Japan). The H_2O_2 generation rate was measured in non-phosphorylating conditions (=State 4) using either pyruvate/malate or succinate as respiratory substrates. Mitochondria were incubated at 0.1 mg/ml in respiration buffer. All incubations also contained 5 μM Amplex Red, 2 U/ml horseradish peroxidase and 8 U/ml superoxide dismutase. The reaction was initiated by addition of 5 mM succinate or 4 mM pyruvate + 1 mM malonate and the increase in fluorescence was followed at excitation and emission wavelengths of 560 and 590 nm, respectively. Appropriate correction for background signals and standard curves generated using known amounts of H_2O_2 were used to calculate the rate of H_2O_2 production in nmol/min/mg mitochondrial protein. The percentage free radical leak, which is a measure of the number of electrons that produce superoxide (and subsequently H_2O_2) compared with the total number of electrons which pass thorough the respiratory chain, was calculated as the rate of H_2O_2 production divided by the rate of O_2 consumption (Barja et al., 1994).

Statistics

Values are presented as means ± SEM except Fig. 2D, in which error bars indicate SD. The significance of differences between means was assessed by the unpaired Student's *t*-test using Microsoft Excel; *P* values < 0.05 were taken to be significant.

Results

Cell growth and mitochondrial morphology

In general, cultured cells gain their energy mostly from glycolysis. Therefore, cells deficient in respiratory function can grow in normal medium, although possibly at a slower rate, relying predominantly on glycolysis (Hofhaus et al., 1996). Actually, ρ^0 cells, which lack mitochondrial DNA completely, can grow producing energy exclusively through glycolysis (King and Attardi, 1989). On the other hand, galactose metabolism via glycolysis is much slower than glucose metabolism (Reitzer et al., 1979). Therefore, cells in galactose medium are forced to oxidize pyruvate through the mitochondrial respiratory chain for energy required for growth. Consequently, cells with defects in their mitochondrial respiratory chains show growth impairments in galactose medium. To evaluate this phenomenon is also observed in our cells, we examined growth retardation by addition of mitochondrial complex I inhibitor, rotenone (Fig. 1A). In glucose medium, 10 nM rotenone had only a slight effect on the growth of PINK1$^{+/+}$ MEFs and slower growth was observed even in the presence of 100 nM rotenone. However, in the galactose medium, 10 nM rotenone significantly inhibited the growth of PINK1$^{+/+}$ MEFs and 100 nM roteone completely arrested the growth. Therefore, we could confirm that the growth impairment of our cells in the galactose medium was due to mitochondrial respiratory chain defects.

PINK1 acts upstream of parkin, regulating mitochondrial integrity and function; therefore, loss of PINK1 is considered to affect mitochondrial functions. To assess the mitochondrial functions of PINK1$^{-/-}$ MEFs, growth capability in a medium in which galactose replaced glucose was examined. As shown in Fig. 1B, PINK1$^{-/-}$ MEFs appeared to show clear growth impairments in the galactose medium, whereas PINK1$^{+/+}$ MEFs grew slightly slower than in the glucose medium.

No differences of mitochondrial morphology between PINK1$^{+/+}$ and $^{-/-}$ MEFs in the glucose medium were detected (Fig. 1C), consistent with the previous report (Matsuda et al., 2010). However, in the galactose medium, mitochondria of the PINK1$^{-/-}$ MEFs were more fragmented compared to the PINK$^{+/+}$ MEFs (Fig. 1C). This is consistent with previous reports, which found mitochondrial morphological changes were more pronounced when PINK1 knock-down HeLa cells were grown in low-glucose medium (Exner et al., 2007) and human PINK1 homozygous mutant fibroblast in galactose medium (Grünewald et al., 2009). In these cells, mitochondrial morphological changes were associated with the mitochondrial functional impairment.

Assessments of mitochondrial functions at the cellular level

Because PINK1$^{-/-}$ MEFs showed severe growth impairments in the galactose medium, the mitochondrial functions of these cells were assessed at the cellular level. First, cellular respiration rates were measured (Fig. 2A). The basal respiration rate was significantly reduced in PINK1$^{-/-}$ cells compared with that in PINK1$^{+/+}$ cells (11.13 ± 0.71 versus 14.36 ± 1.01 nmol O/min/10^6 cells; $p<0.05$; $n=5$ independent experiments), consistent with previous reports using partial knock-down of PINK1 expression (Gandhi et al., 2009; Liu et al., 2009). Oligomycin inhibits ATP synthase, resulting in non-phosphorylating respiration. FCCP uncouples oxidative phosphorylation, leading to maximum respiration rates. In both conditions, the

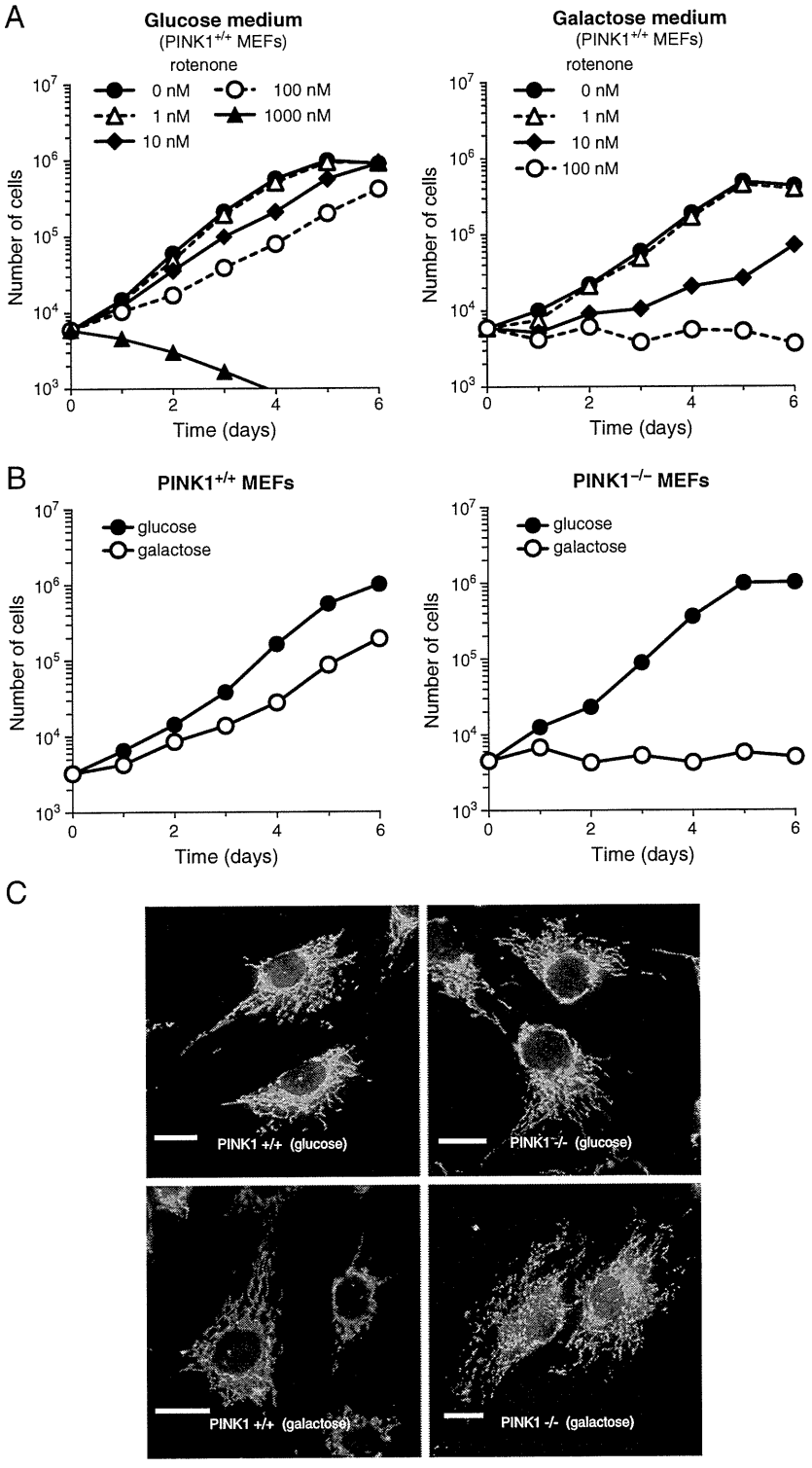

Fig. 1. (A) Growth retardation of PINK1$^{+/+}$ MEFs by mitochondrial complex I inhibitor, rotenone in glucose or galactose medium. Closed circles with solid line, 0 nM rotenone; open triangles with dashed line, 1 nM rotenone; closed diamonds with solid line, 10 nM rotenone; open circles with dashed line, 100 nM rotenone; closed triangles with solid line, 1000 nM rotenone. Cells grown in 12-well plates were trypsinized and live cells were assessed by trypan blue dye exclusion. (B) Growth curves of PINK1$^{+/+}$ and $^{-/-}$ MEFs. Closed symbols (*glucose*), growth curve for cells grown in DMEM containing 4.5 g/l glucose and 1 mM sodium pyruvate; open symbols (*galactose*), growth curve for cells grown in DMEM lacking glucose and containing instead 1.0 g/l galactose and 1 mM sodium pyruvate. Cells grown in 12-well plates were trypsinized and live cells were assessed by trypan blue dye exclusion. (C) Mitochondrial morphology of PINK1$^{+/+}$ and $^{-/-}$ MEFs. After incubating cells with the glucose or galactose medium for 24 hours, cells were fixed and immunostained with anti-Tom20 antibody to visualize mitochondria. Scale bar, 20 μm.

PINK1$^{-/-}$ cells respired significantly slower than the PINK1$^{+/+}$ cells (1.76 ± 0.13 versus 2.95 ± 0.27 ($p<0.01$; $n=5$ independent experiments) and 16.44 ± 1.80 versus 23.50 ± 1.18 nmol O/min/10^6 cells ($p<0.05$; $n=5$ independent experiments), respectively).

The main function of mitochondria is ATP synthesis via oxidative phosphorylation. ATP levels under basal conditions were significantly reduced in PINK1$^{-/-}$ MEFs (Fig. 2B), as reported previously for dissociated PINK1$^{-/-}$ mouse neurons (Gispert et al., 2009) and PINK1

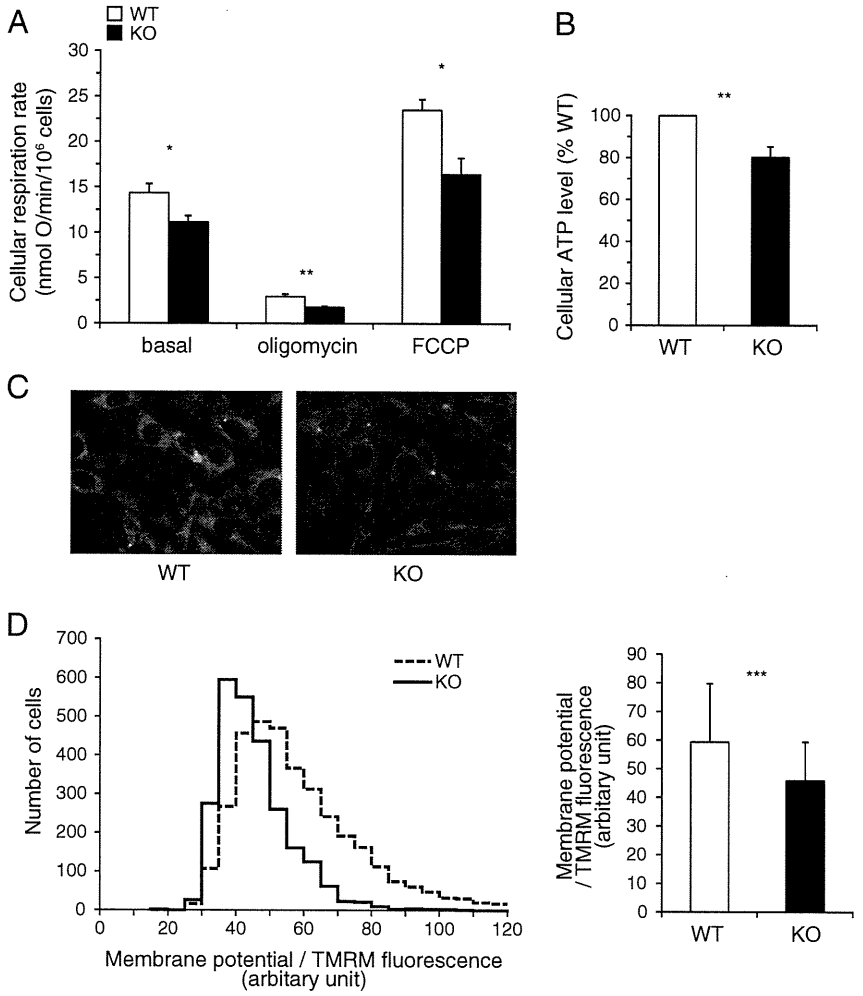

Fig. 2. Mitochondrial functions assessed at the cellular level. Open bars, PINK1$^{+/+}$ MEFs; closed bars, PINK1$^{-/-}$ MEFs. (A) Cell respiration rate of PINK1$^{+/+}$ and $^{-/-}$ MEFs. The oxygen respiration rate was measured at density of 8.0×10^6 cells/ml under each of the following three conditions: basal rate (no additions); State 4 (no ATP synthesis) [after addition of 1 μg/ml oligomycin], uncoupled [after addition of 3 μM FCCP]. After sequential measurements, the endogenous respiration rate was determined by adding 1 μM rotenone + 2 μM myxothiazol. Error bars indicate SEM ($n = 5$ independent experiments). (B) Cellular ATP levels. Data were normalized based on cell numbers and expressed as the percentage of the level in PINK1$^{+/+}$ cells. Error bars indicate SEM ($n = 4$ independent experiments). (C) Live cell images of PINK1$^{+/+}$ and $^{-/-}$ MEFs with TMRM fluorescence. (D) Mitochondrial membrane potential evaluated by live cell imaging of TMRM fluorescence. *Left panel*, the distribution of TMRM fluorescence from 3537 PIINK1$^{+/+}$ and 2566 PINK1$^{-/-}$ cells from 12 wells per cell type; *right panel*, the average value of TMRM fluorescence per cell. Error bars indicate SD. *$P<0.05$; **$P<0.01$; ***$P<0.001$.

siRNA knock-down PC12 cells (Liu et al., 2009). Mitochondrial membrane potential was also measured by live cell imaging of TMRM fluorescence. Typical images were shown in Fig. 2C. The histogram shows the distribution of TMRM fluorescence from 3537 PINK1$^{+/+}$ cells and 2566 PINK1$^{-/-}$ cells from 12 wells per cell type and the bar graph indicates the mean ± SD of TMRM fluorescence per cell (Fig. 2D). According to the Nernst equation, the ratio of TMRM fluorescence would translate into, on average, 6.88 mV lower mitochondrial membrane potential in the PINK1$^{-/-}$ cells if the plasma membrane potentials were not different between PINK1$^{+/+}$ and $^{-/-}$ cells. Mitochondrial membrane potential decrease was also showed previously in PINK1 knock-down HeLa cells (Exner et al., 2007) and in stable PINK1 knock-down neuroblastoma cell lines (Sandebring et al., 2009).

Assessments of mitochondrial functions using isolated mitochondria

To further analyze mitochondrial functions, we measured the kinetics of oxidative phosphorylation using isolated mitochondria from PINK1$^{+/+}$ and $^{-/-}$ MEFs. Fig. 3 shows the kinetics of the three modules of oxidative phosphorylation using succinate as a respiratory substrate (complex II-linked respiration). Fig. 3A shows the kinetic response of substrate oxidation to its product, $\Delta\psi$. The substrate oxidation kinetic curve for PINK1$^{-/-}$ cells was clearly shifted lower compared with that for PINK1$^{+/+}$ cells, indicating that the loss of PINK1 caused mitochondrial respiratory chain defects. Fig. 3B shows the kinetic response of proton leak to its driving force, $\Delta\psi$, and Fig. 3C shows the kinetic response of the ATP phosphorylating pathway to its driving force, $\Delta\psi$. Both kinetic curves for PINK1$^{+/+}$ and $^{-/-}$ MEFs (open and closed symbols, respectively) were overlapping, implying that there were no significant differences in those modules.

We also independently measured the mitochondrial oxygen consumption rate using pyruvate/malate as a respiratory substrate instead of succinate to check complex I. Modular kinetic analysis using pyruvate/malate is technically difficult for the following reasons: (1) the oxygen consumption rate with pyruvate/malate is much slower than succinate respiration; and (2) there are no competitive inhibitors of complex I-linked respiration, such as malonate for succinate respiration. As shown in Fig. 4A, the respiration rates in State 3 and 4 with pyruvate/malate of isolated mitochondria from PINK1$^{-/-}$ cells (closed symbols) were significantly slower than those of PINK1$^{+/+}$ cells (open symbols), as in the case of succinate respiration (Fig. 4B; data derived from the kinetic curves in Fig. 3).

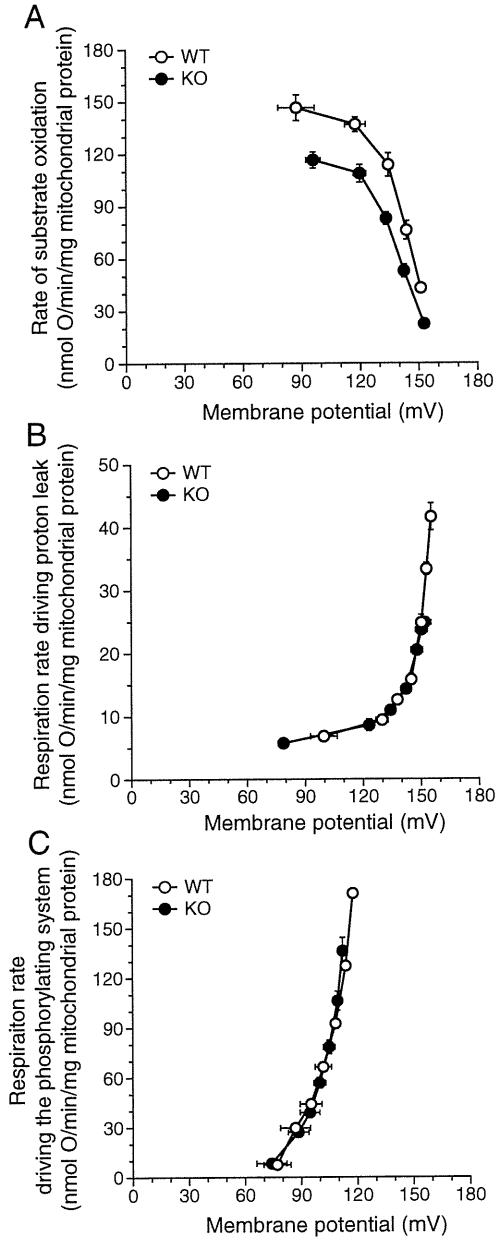

Fig. 3. Modular kinetic analysis of oxidative phosphorylation in mitochondria isolated from PINK1$^{+/+}$ and $^{-/-}$ MEFs. Modular kinetic analysis of the kinetic responses to membrane potential, $\Delta\psi$, of respiration driving (A) substrate oxidation ($\Delta\psi$ titrated with uncoupler, FCCP, starting in State 4), (B) proton leak ($\Delta\psi$ titrated with malonate, starting in State 4) and (C) the phosphorylating system, calculated by subtracting respiration driving proton leak from respiration driving the $\Delta\psi$-consumers ($\Delta\psi$ titrated with malonate starting in State 3; not shown) at each $\Delta\psi$. Open symbols, PINK1$^{+/+}$ MEFs; closed symbols, PINK1$^{-/-}$ MEFs. Error bars indicate SEM ($n=4$ independent mitochondrial preparations).

Mitochondrial ROS production

Mitochondrial ROS production rate was assessed by measurement of the H_2O_2 generation rate. Mechanisms of mitochondrial ROS production were well described elsewhere (Fig. 1 of Lambert et al., 2010). Pyruvate and malate generate NADH, which induced forward electron transport and generate ROS mainly from complex I and III. For pyruvate/malate respiration, the basal H_2O_2 generation rate (measured in the absence of respiratory chain inhibitors) was not different between PINK1$^{+/+}$ and $^{-/-}$ mitochondria (Fig. 4C). The addition of antimycin A and further addition of rotenone, which inhibited forward electron transport at complex III and I, respectively, enhanced H_2O_2 generation. During succinate respiration in the absence of respiratory chain inhibitors, ROS are generated mainly from the quinine binding site of complex I due to reverse electron flow from coenzyme Q to complex I. For succinate respiration, H_2O_2 generation rate in the absence of reparatory chain inhibitors was higher in PINK1$^{+/+}$ mitochondria than in PINK1$^{-/-}$ mitochondria, but the difference was not significant (Fig. 4D). The addition of rotenone, which blocks reverse electron flow from coenzyme Q to complex I, attenuated H_2O_2 generation.

Figs. 4 C and D show a tendency for PINK1$^{+/+}$ mitochondria to generate more ROS than PINK1$^{-/-}$ mitochondria. However, their respiration rates were remarkably different (Figs. 4A and B). Therefore, we calculated the percentage free radical leak, which is the fraction of molecules of O_2 consumed that give rise to H_2O_2 release by mitochondria (free radical leak) during either pyruvate/malate or succinate State 4 respiration (Figs. 4E and F). For pyruvate/malate respiration, mitochondria isolated from PINK1$^{-/-}$ cells had higher proportion of H_2O_2 generation than PINK1$^{+/+}$ mitochondria. During succinate respiration without respiratory inhibitors, PINK1$^{-/-}$ mitochondria had also higher proportion of free radical leak mainly from complex I due to reverse electron flow from coenzyme Q to complex I. Because the differences disappeared with addition of rotenone, which inhibit reverse electron flow, ROS generation enhanced by loss of PINK1 was mostly from complex I.

Discussion

We produced an *in vitro* model of Parkinson's disease, immortalized PINK1$^{-/-}$ MEFs. Previously, impairment of mitochondrial respiration was observed in the brains of PINK1$^{-/-}$ mice (Gautier et al., 2008). PINK1$^{-/-}$ MEFs clearly showed a phenotype of mitochondrial dysfunctions, which is consistent with PD pathogenesis. This phenotype was apparent in a cell growth experiment using medium containing galactose instead of glucose (Fig. 1B). Mitochondrial fragmentation was observed when PINK1$^{-/-}$ MEFs grew in the galactose medium (Fig. 1C), which was consistent with previous reports (Exner et al., 2007; Grünewald et al., 2009). Our results have unveiled that the PINK1$^{-/-}$ MEF line could be a potential PD model, presenting growth retardation due to decreased mitochondrial respiration activity. Thus, the PINK1$^{-/-}$ MEFs are a useful tool for evaluating the role of PINK1 in mitochondrial dysfunction and relevant to PD.

In PINK1$^{-/-}$ MEFs, mitochondrial membrane potential was decreased compared with that in littermate wild-type MEFs (Figs. 2C and D), as reported previously for PINK1 knock-down HeLa cells (Exner et al., 2007) and stable PINK1 knock-down neuroblastoma cell lines (Sandebring et al., 2009). This is a key event during elimination of mitochondria. Mitochondrial fission followed by selective fusion segregates damaged mitochondria, which decreases their membrane potential, and permits their removal by autophagy (Twig et al., 2008). The PINK1–parkin pathway is thought to have a crucial role in this mitochondrial elimination mechanism (Geisler et al., 2010; Kawajiri et al., 2010; Matsuda et al., 2010; Narendra et al., 2008, 2010; Vives-Bauza et al., 2010). To clarify what caused the decrease in mitochondrial membrane potential, we performed a modular kinetic analysis using isolated mitochondria (Fig. 3). This analyzes the kinetics of the whole of oxidative phosphorylation divided into three modules connected by their common substrate or product, mitochondrial membrane potential ($\Delta\psi$). The modules are include one $\Delta\psi$-producer (substrate oxidation) and two $\Delta\psi$-consumers (phosphorylating system and proton leak) (Brand, 1990). To decrease $\Delta\psi$, the $\Delta\psi$-producer should be down-regulated and/or $\Delta\psi$-consumers should be up-regulated. As cellular ATP levels were decreased compared with those in littermate wild-type MEFs (Fig. 2B), it is unlikely that the phosphorylating system is up-regulated. Indeed, the kinetics of the phosphorylation module were not altered (Fig. 3C). The other $\Delta\psi$-consumer, proton leak,

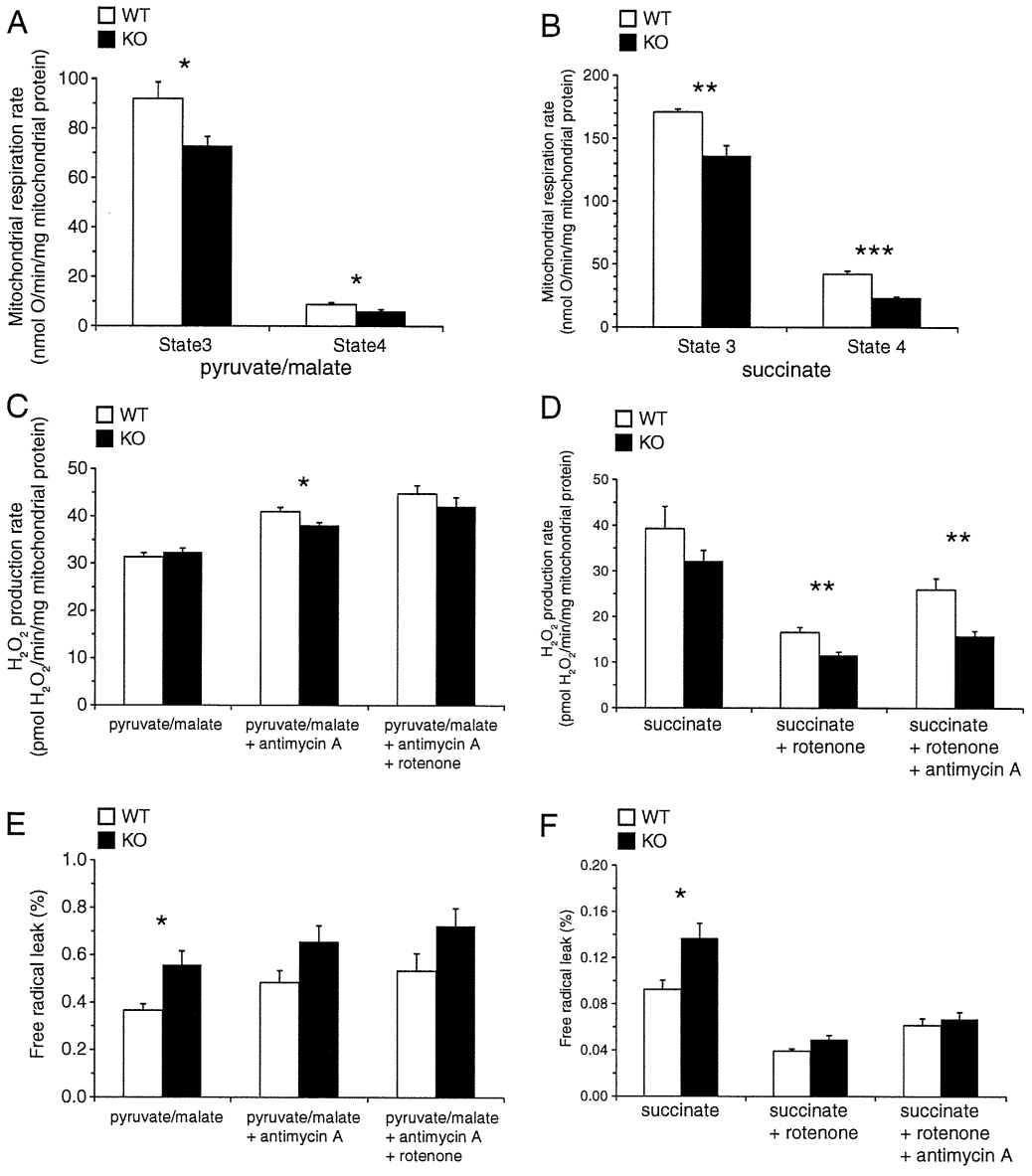

Fig. 4. Oxygen consumption rate and H_2O_2 production rate of mitochondria isolated from PINK1$^{+/+}$ and $^{-/-}$ MEFs. Open bars, PINK1$^{+/+}$ MEFs; closed bars, PINK1$^{-/-}$ MEFs. (A) State 3 and State 4 respiration rate of mitochondria with pyruvate/malate as a respiratory substrate. (B) State 3 and State 4 respiration rate of mitochondria with succinate as a respiratory substrate. Data were derived from the results of modular kinetic analysis (Fig. 3). State 3 respiration rates were the kinetic start points of the $\Delta\psi$-consumers (the sum of the phosphorylating system and proton leak). State 4 respiration rates were average values of the respiration rates at the kinetic start points of substrate oxidation and proton leak. (C, D) Mitochondrial H_2O_2 production rate with pyruvate/malate (C) or succinate (D) as a respiratory substrate. (E, F) Percentage free radical leak (FRL) for State 4 respiration with pyruvate/malate (E) or succinate (F) as a respiratory substrate. Error bars indicate SEM ($n=5$ and 4 independent mitochondrial preparations for pyruvate/malate and succinate respiration, respectively). *$P<0.05$; **$P<0.01$; ***$P<0.001$.

which partially dissipates the membrane potential without ATP synthesis, was also not changed (Fig. 3B). Therefore, the decrease in membrane potential caused by loss of PINK1 is likely to have been caused only by lower activity of the $\Delta\psi$-producer, substrate oxidation (Fig. 3A). This is the first report showing that mitochondrial membrane potential decrease caused by loss of PINK1, which is the key event for the following mitochondrial elimination, was not due to proton leak, but to respiratory chain defects. We used only succinate (a complex II-linked substrate) as a respiratory substrate in the modular kinetic analysis for technical reasons. However, complex I-linked respiration (pyruvate/malate) was also decreased in PINK1$^{-/-}$ MEFs like succinate respiration (Fig. 4A).

The mitochondrial respiration rates in State 4 were decreased in PINK1$^{-/-}$ MEFs, and consequently, the proportions of free radical leak were significantly higher in PINK1$^{-/-}$ MEFs than in PINK1$^{+/+}$ MEFs (Figs. 4E and F). Because the differences disappeared with addition of rotenone (complex I inhibitor, which inhibits reverse electron flow from coenzyme Q to complex I), ROS generation enhanced by loss of PINK1 was mostly from complex I. These results are partially consistent with those in previous reports, suggesting that MPTP and rotenone induce neuronal cell death by inhibiting complex I activity, leading to a PD-like phenotype (Dauer and Przedborski, 2003; Jackson-Lewis and Przedborski, 2007; Trojanowski, 2003).

In this study, we developed an *in vitro* PD model, the PINK1$^{-/-}$ MEF line, and established the experimental conditions for cell growth to detect mitochondrial dysfunction. This is the first report showing that complete ablation of PINK1 causes a decrease in mitochondrial membrane potential, which is not due to proton leak, but to respiratory chain defects.

Supplementary materials related to this article can be found online at doi:10.1016/j.nbd.2010.08.027.

Acknowledgments

This work was supported by a Grant-in-Aid for Scientific Research for Young Scientists (B) from JSPS (T.A. and S.Saiki), a JSPS fellowship (T.A.), Nagao Memorial Fund (S. Saiki) and a Grant from Takeda Scientific Foundation (S. Saiki and T.A.). We thank Dr. Noriyuki Matsuda for assistance to obtain immortalized cells.

References

Abou-Sleiman, P.M., Muqit, M.M., Wood, N.W., 2006. Expanding insights of mitochondrial dysfunction in Parkinson's disease. Nat. Rev. Neurosci. 7, 207–219.

Amo, T., Brand, M.D., 2007. Were inefficient mitochondrial haplogroups selected during migrations of modern humans? A test using modular kinetic analysis of coupling in mitochondria from cybrid cell lines. Biochem. J. 404, 345–351.

Barja, G., Cadenas, S., Rojas, C., Pérez-Campo, R., López-Torres, M., 1994. Low mitochondrial free radical production per unit O_2 consumption can explain the simultaneous presence of high longevity and high aerobic metabolic rate in birds. Free Radic. Res. 21, 317–327.

Brand, M.D., 1990. The proton leak across the mitochondrial inner membrane. Biochim. Biophys. Acta 1018, 128–133.

Brand, M.D., 1995. Measurement of mitochondrial protonmotive force. In: Brown, G.C., Cooper, C.E. (Eds.), Bioenergetics, a practical approach. IRL Press, Oxford, pp. 39–62.

Brand, M.D., 1998. Top-down elasticity analysis and its application to energy metabolism in isolated mitochondria and intact cells. Mol. Cell. Biochem. 184, 13–20.

Brand, M.D., Chien, L.F., Diolez, P., 1994. Experimental discrimination between proton leak and redox slip during mitochondrial electron transport. Biochem. J. 297, 27–29.

Chu, C.T., 2010. Tickled PINK1: mitochondrial homeostasis and autophagy in recessive Parkinsonism. Biochim. Biophys. Acta 1802, 20–28.

Clark, I.E., Dodson, M.W., Jiang, C., Cao, J.H., Huh, J.R., Seol, J.H., Yoo, S.J., Hay, B.A., Guo, M., 2006. *Drosophila pink1* is required for mitochondrial function and interacts genetically with *parkin*. Nature 441, 1162–1166.

Dauer, W., Przedborski, S., 2003. Parkinson's disease: mechanisms and models. Neuron 39, 889–909.

Exner, N., Treske, B., Paquet, D., Holmstrom, K., Schiesling, C., Gispert, S., Carballo-Carbajal, I., Berg, D., Hoepken, H.H., Gasser, T., Krüger, R., Winklhofer, K.F., Vogel, F., Reichert, A.S., Auburger, G., Kahle, P.J., Schmid, B., Haass, C., 2007. Loss-of-function of human PINK1 results in mitochondrial pathology and can be rescued by parkin. J. Neurosci. 27, 12413–12418.

Gandhi, S., Wood-Kaczmar, A., Yao, Z., Plun-Favreau, H., Deas, E., Klupsch, K., Downward, J., Latchman, D.S., Tabrizi, S.J., Wood, N.W., Duchen, M.R., Abramov, A.Y., 2009. PINK1-associated Parkinson's disease is caused by neuronal vulnerability to calcium-induced cell death. Mol. Cell 33, 627–638.

Gautier, C.A., Kitada, T., Shen, J., 2008. Loss of PINK1 causes mitochondrial functional defects and increased sensitivity to oxidative stress. Proc. Natl. Acad. Sci. U. S. A. 105, 11364–11369.

Geisler, S., Holmström, K.M., Skujat, D., Fiesel, F.C., Rothfuss, O.C., Kahle, P.J., Springer, W., 2010. PINK1/Parkin-mediated mitophagy is dependent on VDAC1 and p62/SQSTM1. Nat. Cell Biol. 12, 119–131.

Gispert, S., Ricciardi, F., Kurz, A., Azizov, M., Hoepken, H.H., Becker, D., Voos, W., Leuner, K., Müller, W.E., Kudin, A.P., Kunz, W.S., Zimmermann, A., Roeper, J., Wenzel, D., Jendrach, M., García-Arencíbia, M., Fernández-Ruiz, J., Huber, L., Rohrer, H., Barrera, M., Reichert, A.S., Rüb, U., Chen, A., Nussbaum, R.L., Auburger, G., 2009. Parkinson phenotype in aged PINK1-deficient mice is accompanied by progressive mitochondrial dysfunction in absence of neurodegeneration. PLoS One 4, e5777.

Grünewald, A., Gegg, M.E., Taanman, J.W., King, R.H., Kock, N., Klein, C., Schapira, A.H., 2009. Differential effects of PINK1 nonsense and missense mutations on mitochondrial function and morphology. Exp. Neurol. 219, 266–273.

Haque, M.E., Thomas, K.J., D'Souza, C., Callaghan, S., Kitada, T., Slack, R.S., Fraser, P., Cookson, M.R., Tandon, A., Park, D.S., 2008. Cytoplasmic Pink1 activity protects neurons from dopaminergic neurotoxin MPTP. Proc. Natl. Acad. Sci. U. S. A. 105, 1716–1721.

Hofhaus, G., Johns, D.R., Hurko, O., Attardi, G., Chomyn, A., 1996. Respiration and growth defects in transmitochondrial cell lines carrying the 11778 mutation associated with Leber's hereditary optic neuropathy. J. Biol. Chem. 271, 13155–13161.

Jackson-Lewis, V., Przedborski, S., 2007. Protocol for the MPTP mouse model of Parkinson's disease. Nat. Protoc. 2, 141–151.

Kawajiri, S., Saiki, S., Sato, S., Sato, F., Hatano, T., Eguchi, H., Hattori, N., 2010. PINK1 is recruited to mitochondria with parkin and associates with LC3 in mitophagy. FEBS Lett. 584, 1073–1079.

Kim, Y., Park, J., Kim, S., Song, S., Kwon, S.K., Lee, S.H., Kitada, T., Kim, J.M., Chung, J., 2008. PINK1 controls mitochondrial localization of Parkin through direct phosphorylation. Biochem. Biophys. Res. Commun. 377, 975–980.

King, M.P., Attardi, G., 1989. Human cells lacking mtDNA: repopulation with exogenous mitochondria by complementation. Science 246, 500–503.

Lambert, A.J., Buckingham, J.A., Boysen, H.M., Brand, M.D., 2010. Low complex I content explains the low hydrogen peroxide production rate of heart mitochondria from the long-lived pigeon, Columba livia. Aging Cell 9, 78–91.

Liu, W., Vives-Bauza, C., Acin-Perez, R., Yamamoto, A., Tan, Y., Li, Y., Magrane, J., Stavarache, M.A., Shaffer, S., Chang, S., Kaplitt, M.G., Huang, X.Y., Beal, M.F., Manfredi, G., Li, C., 2009. PINK1 defect causes mitochondrial dysfunction, proteasomal deficit and alpha-synuclein aggregation in cell culture models of Parkinson's disease. PLoS One 4, e4597.

Matsuda, N., Sato, S., Shiba, K., Okatsu, K., Saisho, K., Gautier, C.A., Sou, Y.S., Saiki, S., Kawajiri, S., Sato, F., Kimura, M., Komatsu, M., Hattori, N., Tanaka, K., 2010. PINK1 stabilized by mitochondrial depolarization recruits Parkin to damaged mitochondria and activates latent Parkin for mitophagy. J. Cell Biol. 189, 211–221.

Narendra, D., Tanaka, A., Suen, D.F., Youle, R.J., 2008. Parkin is recruited selectively to impaired mitochondria and promotes their autophagy. J. Cell Biol. 183, 795–803.

Narendra, D.P., Jin, S.M., Tanaka, A., Suen, D.F., Gautier, C.A., Shen, J., Cookson, M.R., Youle, R.J., 2010. PINK1 is selectively stabilized on impaired mitochondria to activate Parkin. PLoS Biol. 8, e1000298.

Park, J., Lee, S.B., Lee, S., Kim, Y., Song, S., Kim, S., Bae, E., Kim, J., Shong, M., Kim, J.M., Chung, J., 2006. Mitochondrial dysfunction in *Drosophila PINK1* mutants is complemented by *parkin*. Nature 441, 1157–1161.

Pridgeon, J.W., Olzmann, J.A., Chin, L.S., Li, L., 2007. PINK1 protects against oxidative stress by phosphorylating mitochondrial chaperone TRAP1. PLoS Biol. 5, e172.

Reitzer, L.J., Wice, B.M., Kennell, D., 1979. Evidence that glutamine, not sugar, is the major energy source for cultured HeLa cells. J. Biol. Chem. 254, 2669–2676.

Reynafarje, B., Costa, L.E., Lehninger, A.L., 1985. O_2 solubility in aqueous media determined by a kinetic method. Anal. Biochem. 145, 406–418.

Sandebring, A., Thomas, K.J., Beilina, A., van der Brug, M., Cleland, M.M., Ahmad, R., Miller, D.W., Zambrano, I., Cowburn, R.F., Behbahani, H., Cedazo-Mínguez, A., Cookson, M.R., 2009. Mitochondrial alterations in PINK1 deficient cells are influenced by calcineurin-dependent dephosphorylation of dynamin-related protein 1. PLoS One 4, e5701.

Trojanowski, J.Q., 2003. Rotenone neurotoxicity: a new window on environmental causes of Parkinson's disease and related brain amyloidoses. Exp. Neurol. 179, 6–8.

Twig, G., Elorza, A., Molina, A.J., Mohamed, H., Wikstrom, J.D., Walzer, G., Stiles, L., Haigh, S.E., Katz, S., Las, G., Alroy, J., Wu, M., Py, B.F., Yuan, J., Deeney, J.T., Corkey, B. E., Shirihai, O.S., 2008. Fission and selective fusion govern mitochondrial segregation and elimination by autophagy. EMBO J. 27, 433–446.

Valente, E.M., Abou-Sleiman, P.M., Caputo, V., Muqit, M.M., Harvey, K., Gispert, S., Ali, Z., Del Turco, D., Bentivoglio, A.R., Healy, D.G., Albanese, A., Nussbaum, R., González-Maldonado, R., Deller, T., Salvi, S., Cortelli, P., Gilks, W.P., Latchman, D.S., Harvey, R.J., Dallapiccola, B., Auburger, G., Wood, N.W., 2004. Hereditary early-onset Parkinson's disease caused by mutations in *PINK1*. Science 304, 1158–1160.

Vives-Bauza, C., Zhou, C., Huang, Y., Cui, M., de Vries, R.L., Kim, J., May, J., Tocilescu, M.A., Liu, W., Ko, H.S., Magrane, J., Moore, D.J., Dawson, V.L., Grailhe, R., Dawson, T.M., Li, C., Tieu, K., Przedborski, S., 2010. PINK1-dependent recruitment of Parkin to mitochondria in mitophagy. Proc. Natl. Acad. Sci. U. S. A. 107, 378–383.

Wood-Kaczmar, A., Gandhi, S., Yao, Z., Abramov, A.Y., Miljan, E.A., Keen, G., Stanyer, L., Hargreaves, I., Klupsch, K., Deas, E., Downward, J., Mansfield, L., Jat, P., Taylor, J., Heales, S., Duchen, M.R., Latchman, D., Tabrizi, S.J., Wood, N.W., 2008. PINK1 is necessary for long term survival and mitochondrial function in human dopaminergic neurons. PLoS One 3, e2455.

Yang, Y., Ouyang, Y., Yang, L., Beal, M.F., McQuibban, A., Vogel, H., Lu, B., 2008. Pink1 regulates mitochondrial dynamics through interaction with the fission/fusion machinery. Proc. Natl. Acad. Sci. U. S. A. 105, 7070–7075.

BASIC RESEARCH PAPER

Autophagy 7:2, 1-12; February 2011; © 2011 Landes Bioscience

Caffeine induces apoptosis by enhancement of autophagy via PI3K/Akt/mTOR/p70S6K inhibition

Shinji Saiki,[1] Yukiko Sasazawa,[2] Yoko Imamichi,[1] Sumihiro Kawajiri,[1] Takahiro Fujimaki,[2] Isei Tanida,[3] Hiroki Kobayashi,[2] Fumiaki Sato,[4] Shigeto Sato,[1] Kei-Ichi Ishikawa,[1] Masaya Imoto[2] and Nobutaka Hattori[1,*]

[1]Department of Neurology; Juntendo University School of Medicine; Bunkyo, Tokyo; [2]Department of Biosciences and Informatics; Faculty of Science and Technology; Keio University; Kohoku, Yokohama; [3]Department of Biochemistry and Cell Biology; National Institute of Infectious Diseases; Shinjyuku, Tokyo; [4]Research Institute for Disease of Old Age; Juntendo University School of Medicine; Tokyo, Japan

Key words: apoptosis, autophagy, PI3K/Akt/mTOR/p70S6K, ERK1/2, caffeine

Abbreviations: PI3K, phosphoinositide-3 kinase; 4E-BP1, eukaryotic initiation factor 4-binding protein 1; ERK, extracellular signal-regulated kinase; mTOR, mammalian target of rapamycin; 3-MA, 3-methyladenine; MEFs, mouse embryonic fibroblasts; p70S6K, 70-kDa ribosomal protein S6 kinase; PI, propidium iodide; MPP^+, 1-methyl-4-phenylpyridinium

Caffeine is one of the most frequently ingested neuroactive compounds. All known mechanisms of apoptosis induced by caffeine act through cell cycle modulation or p53 induction. It is currently unknown whether caffeine-induced apoptosis is associated with other cell death mechanisms, such as autophagy. Herein we show that caffeine increases both the levels of microtubule-associated protein 1 light chain 3-II and the number of autophagosomes, through the use of western blotting, electron microscopy and immunocytochemistry techniques. Phosphorylated p70 ribosomal protein S6 kinase (Thr389), S6 ribosomal protein (Ser235/236), 4E-BP1 (Thr37/46) and Akt (Ser473) were significantly decreased by caffeine. In contrast, ERK1/2 (Thr202/204) was increased by caffeine, suggesting an inhibition of the Akt/mTOR/p70S6K pathway and activation of the ERK1/2 pathway. Although insulin treatment phosphorylated Akt (Ser473) and led to autophagy suppression, the effect of insulin treatment was completely abolished by caffeine addition. Caffeine-induced autophagy was not completely blocked by inhibition of ERK1/2 by U0126. Caffeine induced reduction of mitochondrial membrane potentials and apoptosis in a dose-dependent manner, which was further attenuated by the inhibition of autophagy with 3-methyladenine or Atg7 siRNA knockdown. Furthermore, there was a reduced number of early apoptotic cells (annexin V positive, propidium iodide negative) among autophagy-deficient mouse embryonic fibroblasts treated with caffeine than in their wild-type counterparts. These results support previous studies on the use of caffeine in the treatment of human tumors and indicate a potential new target in the regulation of apoptosis.

Introduction

Caffeine has a diverse range of pharmacological effects.[1] In addition to its various effects on the cell cycle and growth arrest, higher (4–10 mM) concentrations of caffeine can induce apoptosis in several cell lines, such as 10 mM caffeine in human neuroblastoma cells,[2] 4 mM caffeine in human pancreatic adenocarcinoma cells[3] and 5 mM caffeine in human A549 lung adenocarcinoma cells.[4] Although caffeine has been reported to modulate cell cycle checkpoints and perturb molecular targets of the cell cycle, the exact mechanism of caffeine-induced apoptosis remains unclear.[1]

Autophagy is a key mechanism in various physiopathological processes, including tumorigenesis, development, cell death and survival.[5,6] It has also been shown to have a complex relationship with apoptosis, especially in tumor cell lines.[7] Several reports have shown that autophagy not only enhances caspase-dependent cell death, but is also required for it.[8] In contrast, it has also been shown that autophagy plays an important role in promoting cell survival against apoptosis.[7] Caffeine has been reported to inhibit some kinase activities, including various forms of phosphoinositol-3 kinase and mammalian target of rapamycin (mTOR).[9,10] Recently, in food spoilage studies involving yeast, caffeine has been shown to induce a starvation response,[11] which is a key regulator of autophagy causing its induction. However, the exact mechanism by which caffeine induces autophagy is still unknown.

Here we report that higher concentrations of caffeine enhance autophagic flux in a dose-dependent manner in various cell lines. Furthermore, we show that caffeine-induced autophagy is mainly dependent on PI3K/Akt/mTOR/p70S6 signaling and eventually results in apoptosis.

*Correspondence to: Nobutaka Hattori; Email: nhattori@juntendo.ac.jp
Submitted: 06/22/10; Revised: 10/27/10; Accepted: 11/02/10
Previously published online: www.landesbioscience.com/journals/autophagy/article/14074
DOI:

Results and Discussion

Caffeine (**Fig. 1A**) is a widely used psychoactive drug that has been used for centuries to increase alertness and energy. It has been reported that caffeine induces autophagy in *Zygosaccharomyces bailii* in association with a starvation response, caused by a unknown mechanism.[11] However, it remains unknown whether caffeine affects autophagy in mammalian cells. To determine if caffeine regulates autophagy at a steady state, we first examined levels of the microtubule-associated protein 1 light chain 3 (LC3)-II, which is an LC3-phosphatidyl-ethanolamine conjugate and a promising autophagosomal marker.[12] LC3-II levels (compared to actin loading controls) increased with 5–25 mM caffeine treatment over 48 hours in SH-SY5Y (**Fig. 1B and C**), PC12D and HeLa cells (**Suppl. Fig. S1A and B**). The LC3-II/actin ratio also increased in a time-dependent manner in SH-SY5Y (**Fig. 1D and E**) and HeLa cells (data not shown). Using an electron microscopy technique, the numbers of autophagic vacuoles (AVs) were markedly increased in SH-SY5Y cells treated with 10 or 25 mM caffeine, but not in the control (**Fig. 1F and G**). Morphometric analysis revealed that the number of AVs per 100 μm^2 of SH-SY5Y cytoplasm in control (Mean ± standard deviation: 1.3 ± 0.50), whereas that in caffeine-treated cells (10 mM: 8.0 ± 0.82; 25 mM: 15 ± 1.9) for 24 hours. Expression levels of p62, a well-known autophagic substrate, were also decreased by caffeine treatment in SH-SY5Y (**Fig. 1H and I**) and HeLa cells (**Suppl. Fig. S1C and D**). Furthermore, 10 mM caffeine treatment markedly increased the number of EGFP-LC3-positive vesicles in SH-SY5Y cells transiently transfected with EGFP-LC3 (data not shown) and HeLa cells stably expressing EGFP-LC3 (**Figs. 1J and K**).[12,13] This effect was confirmed by the observation that caffeine administration also increased the number of vesicles positive to endogenous LC3 (**Suppl. Fig. S1E**).

Endogenous LC3 is post-transcriptionally processed into LC3-I, which is found in the cytosol. LC3-I is in turn lipidated to LC3-II, which then associates with autophagosome membranes.[14] LC3-II can accumulate due to increased upstream autophagosome formation or impaired downstream autophagosome-lysosome fusion. To distinguish between these two possibilities, we assayed LC3-II in the presence of E64D plus pepstatin A or bafilomycin A1, which inhibits lysosomal proteases or blocks downstream autophagosome-lysosome fusion and lysosomal proteases, respectively.[15,16] Caffeine significantly increased LC3-II levels in the presence of E64d plus pepstatin A or bafilomycin compared to E64d plus pepstatin A or bafilomycin alone in (**Fig. 2A and B**; **Suppl. Fig. S1F and G**) and HeLa cells (**Fig. 2C and D**; **Suppl. Fig. S1H and I**). A saturating dosage of bafilomycin A1 was used in this assay and no further increases in LC3-II levels were observed when cells were treated with higher concentrations. Similar results were observed in PC12D cell lines (data not shown). To confirm the caffeine effect on autophagic flux, we assessed the numbers of autolysosomes and autophagosomes in HeLa cells. The ratio of the numbers of autolysosomes (positive to both LC3 and LAMP2) to autophagosomes (positive to LC3) was increased by 10 mM caffeine treatment for 48 hours (**Fig. 2E**). Quantification data using ImageJ also showed significant increase of the ratio (**Fig. 2F**). These results strongly indicate that high concentration of caffeine treatment enhances autophagic flux.

The class I phosphatidylinositol 3-phosphate kinase (PI3K)/Akt/mTOR/p70ribosomal protein S6 kinase (p70S6K) signaling pathway and the Ras/Raf-1/mitogen-activated protein kinase 1/2 (MEK1/2)/extracellular signal-regulated kinase 1/2 (ERK1/2) pathway are two well-known pathways involved in the regulation of autophagy. Both are associated with tumorigenesis and often activated in numerous types of tumors.[17] Therefore, we examined the effect of caffeine on both of these pathways, using western blotting, according to the protocol by Inoki and colleagues.[18] After a 24 hour treatment with caffeine, there was a significant decrease in the levels of phosphorylated p70 S6 kinase, S6 ribosomal protein and 4E-BP1, compared with total normal levels in SH-SY5Y (**Fig. 3A**), HeLa and PC12D cells (data not shown). Consistent with these results, nonphosphorylated 4E-BP1 proteins were increased by caffeine treatment (**Fig. 3A**). To further investigate the upstream inhibition of mTOR by caffeine, we examined Ser473 phosphorylation of Akt, which measures both Akt/mTOR and mTORC2 activity. As shown in **Figure 3B**, treatment with caffeine also decreased the level of phosphorylated Akt in SH-SY5Y cells, which was consistent with a previous report.[19] Similar findings were obtained in HeLa (**Suppl. Fig. S2A**) and PC12D cells (data not shown). Subsequently, we examined whether caffeine increases the phosphorylation of ERK1/2, a key regulator of autophagy downstream of Akt. As shown in **Figure 3C**, treatment with caffeine increased phosphorylated ERK1/2. The effects of caffeine on mTOR inhibition were initially detected 3 hours after the addition of caffeine and reached a maximal level after 6 hours in SH-SY5Y (**Fig. 3D**) and 9 hours in HeLa cells (**Suppl. Fig. S2B and C**).

Caffeine has been shown to inhibit PI3K and components of the PI3K/Akt pathway.[9,20] Next, we performed experiments to confirm whether caffeine-induced autophagy is activated through the PI3K/Akt pathway. Insulin or insulin-like growth factor upregulates PI3K and its downstream targets including Akt and mTOR, resulting in the inactivation of autophagy.[21-23] As shown in **Figure 4A and B**, insulin treatment for 30 minutes significantly phosphorylated Akt at Ser473, whereas the phosphorylation was completely abolished by additional treatment with caffeine. No significant differences of the LC3-II/

Figure 1A–G (See opposite page). Caffeine increases autophagic flux in various cell lines. (A) Structural formula of caffeine. (B and C) SH-SY5Y cells treated with various concentrations of caffeine for 24 or 48 hours were analyzed by immunoblotting (B) with antibodies against LC3 and actin. Densitometry analysis of LC3-II levels relative to actin (C) was performed using three independent experiments. (D and E) SH-SY5Y cells treated with 25 mM caffeine for 3–24 hours were analyzed by immunoblotting (D) with antibodies against LC3 and actin. Densitometry analysis of LC3-II levels relative to actin (E) was performed using three independent experiments. (F) Electron microscopic examination of SH-SY5Y cells treated with various concentrations of caffeine for 24 or 48 hours. Autophagic vacuoles accumulating in the cytoplasm are shown by arrows. (G) Morphometric analysis of autophagic vacuoles was performed with 30 different areas of the cytoplasm of control and caffeine-treated cells.

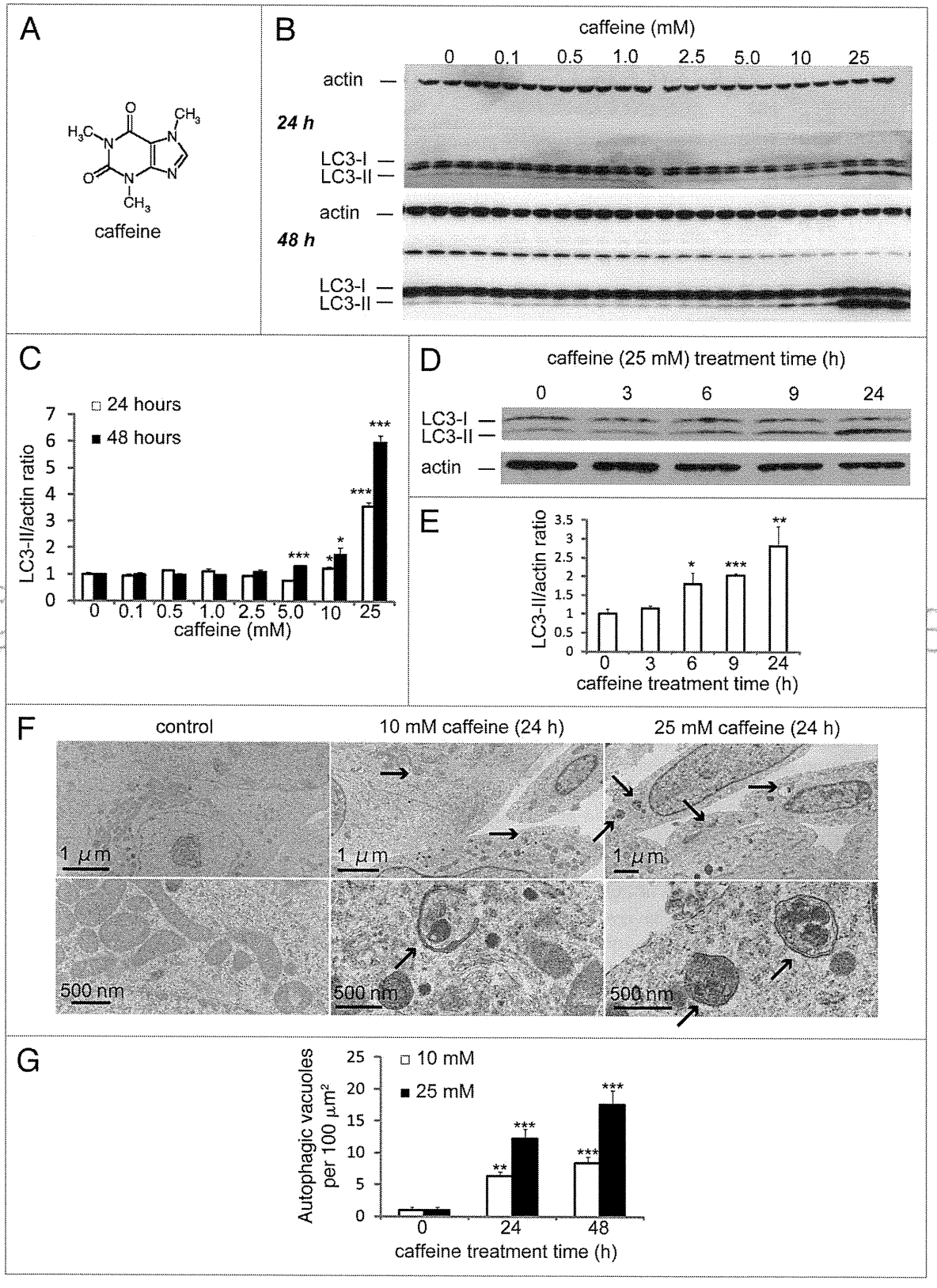

actin ratio between caffeine treatment and caffeine treatment with insulin were observed. Also, caffeine and Akt1/2 inhibitors did not have additive effects on the levels of LC3-II/actin ratio compared to the single treatment of caffeine or Akt inhibitors (**Fig. 4C and D**). To further confirm the caffeine effects on this pathway, cells were transiently transfected with myristoylated Akt (myr-Akt), a constitutively active form of Akt.[24] Caffeine treatment of both cells transfected with control vector and

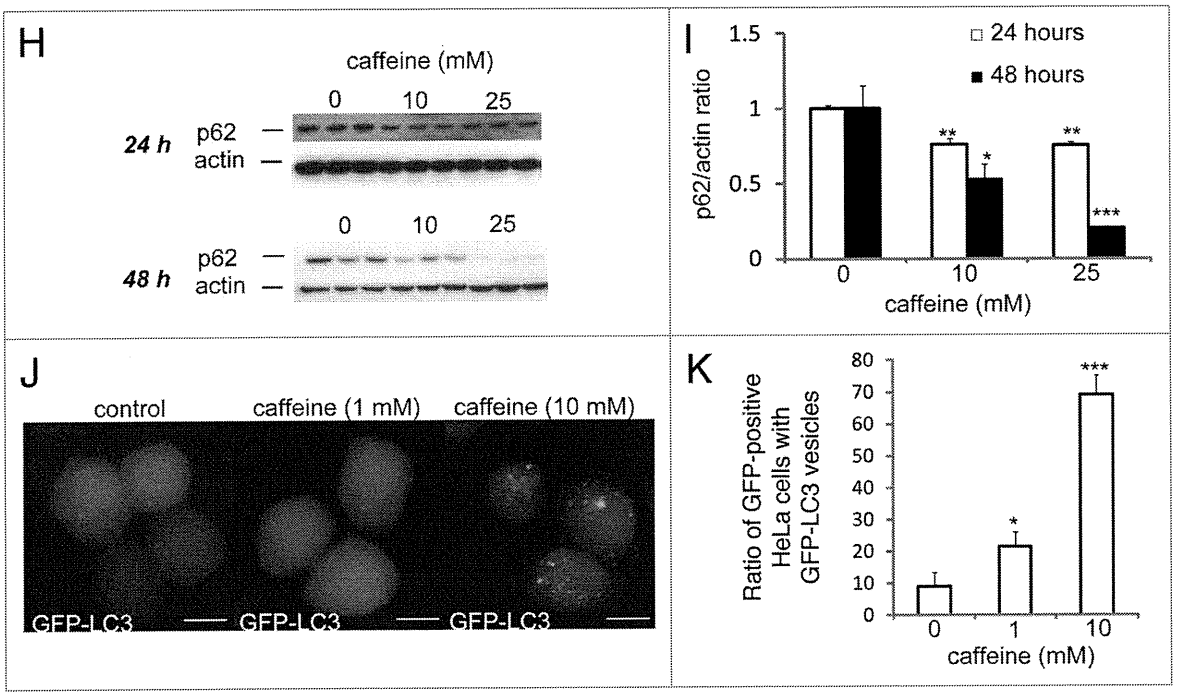

Figure 1H–K. Caffeine increases autophagic flux in various cell lines. (H and I) SH-SY5Y cells treated with various concentrations of caffeine for 24 or 48 hours were analyzed by immunoblotting with antibodies against p62 and actin. Densitometry analysis of p62 levels relative to actin (I) was performed using three independent experiments. (J and K) HeLa cells stably expressing EGFP-LC3 were treated with various concentrations of caffeine for 24 hours and analyzed using confocal microscopy. The percentage of EGFP-positive HeLa cells with >5 EGFP-LC3 vesicles was assessed (K) described previously in reference 43. Error bars, S.D.; *p < 0.05; **p < 0.01.

myr-Akt markedly decreased the levels of the phosphorylated Akt (**Fig. 3E**), indicating that caffeine directly inhibits the Akt phosphorylation. If caffeine facilitates autophagy through PI3K/Akt and ERK1/2 signalings, the autophagy should be partially blocked by ERK1/2 inhibition using the mitogen-activated protein kinase kinase 1/2 (MEK1/2) inhibitor, U0126. U0126 significantly but mildly reversed the levels of LC3-II/actin ratio (**Fig. 4F and G**). The failure of U1026 to reverse completely the caffeine effect can be explained by the autophagy induction through Akt/mTOR signaling. In addition, only Akt knockdown with inducible short hairpin RNAs (shRNAs) to specifically and stably knock down all three Akt isoforms sufficiently increases autophagic flux.[25] Therefore, we concluded that the caffeine-induced autophagy is mainly dependent on the PI3K/Akt/mTOR pathway.

Because caffeine induces autophagy dependently of mTOR inhibition, we hypothesized that combination treatment of caffeine with rapamycin would not have additive effects on autophagy. However, caffeine and rapamycin showed an additive effect on the enhancement of LC3-II/actin ratio compared to the single treatment of caffeine or rapamycin (**Fig. 5A and B**). Several lines of evidences support the hypothesis that resistance to rapamycin results from a positive feedback loop from mTOR/S6K1 to Akt, resulting in enhancement of Akt phosphorylation at Ser 473.[26-28] Recently, mutual suppression of the PI3K/Akt/mTOR pathway by combination of rapamycin with perifosine, an Akt inhibitor, induces synergistic effects on autophagy-induced apoptosis as well as enhancement of autophagy, suggesting that dual inhibition of the PI3K/Akt/mTOR by rapamycin with caffeine would be also a rational treatment for cancer.[29]

Several anti-cancer agents are known to inhibit the PI3K/Akt/mTOR/p70S6K pathway and simultaneously activate ERK1/2, resulting in induction of autophagy in tumor cell lines.[30,31] The upregulation of this process has beneficial effects in neurodegenerative diseases, such as Parkinson and Huntington diseases, whereas an excess of autophagy can lead to cell death.[32,33] Therefore, we decided to investigate whether caffeine-induced autophagy rescues or induces cell death. Using PC12D cells treated with 1-methyl-4-phenylpyridinium (MPP^+), a well-established Parkinson disease model,[34] we determined that 1 mM caffeine treatment was not sufficient for the induction of autophagy (**Suppl. Fig. S4 and B**) and promoted increased cell viability, whereas >2.5 mM caffeine decreased cell viability (**Fig. 6A**). In addition, a significant decrease in cell viability was noted in cells treated with >2.5 mM caffeine without MPP^+. Also, mitochondrial membrane potentials assessed by JC-1 were significantly preserved by 1 mM caffeine treatment compared to the control with MPP^+, while those were lost by >5 mM caffeine treatment (**Fig. 6B and Suppl. Fig. S5A**). These data suggest that caffeine-induced autophagy is not protective in these cell lines and leads to cell death.

Autophagy and apoptosis may act independently in parallel pathways or may influence one another.[7] To confirm the relationship between these pathways in cells treated with caffeine, we examined caffeine effects on the cell cycle with a propidium iodide (PI) staining assay. Treatment with 2.5–10 mM caffeine